

# DIRECT SHAPE FROM ISOPHOTES

V.Dragnea, E.Angelopoulou

Computer Science Department, Stevens Institute of Technology, Hoboken, NJ 07030, USA -  
(vdragnea, elli)@cs.stevens.edu

**KEY WORDS:** Isophotes, Reflectance Map

## ABSTRACT:

This article describes a new method of Shape from Shading, Shape from Isophotes. Shape from Isophotes uses the image isophotes for recovering the object surface normals. It is a propagation method. It initially directly recovers a small number of surface normals and then uses them to estimate normals at neighboring points in either adjacent isophotes or within the same isophote. The propagation can start either from occluding contours or singular points. Shape from Isophotes explicitly addresses brightness quantization errors, which can affect the performance of traditional Shape from Shading techniques. Since our method is based on the relationship between isophote curves and changes in surface normals [9,10], it is mainly applicable to smooth diffuse surfaces. The accuracy of the proposed technique was measured using synthetic images of simple objects with Lambertian reflectance, as well as real objects of known geometry. The normal map was recovered with accuracy of well below 7° average error. The method requires some interpolation, as it is possible that we may not be able to recover the surface normals at each pixel

## 1. INTRODUCTION

There is a big body of work done in the field of Shape from Shading (SFS), [1,2,3,4,5,7,8,11,12,14,15] just to mention a few. Despite their inherent limitations (they often need input images of scenes with strong parallel illumination rays and/or impose object surface restrictions), they are still often used especially for the shape recovery of smooth, featureless surfaces.

Among the first SFS approaches was Horn's use of a set of five differential equations whose solution produces a curve [5], a characteristic strip. The direction of characteristic strips is the direction of the intensity gradients, and in the case of a rotationally symmetric reflectance map they are the curves of steepest descent. Though Horn's characteristic strip technique demonstrated that the recovery of a normal map is feasible from a single image, it may, like most gradient descent methods, produce erroneous results (for more details see section 2.1). Newer algorithms that are still based on gradient descent like Dupuis and Oliensis [3], and Bichsel and Pentland [1] are still suffering from the same limitation.

Other researchers used different techniques to recover the surface normals from intensity images. For example, Kimmel and Bruckstein [8] use level sets for recovering shape from shading. Another class of SFS algorithms treats shape recovery from irradiance as a minimization problem. For example, Horn's [7] minimization approach replaces the smoothness constraint with an integrability constraint. Frankot and Chellappa's [4] minimization approach places emphasis in enforcing integrability. Zheng and Chellappa [15] replace the smoothness constraint with an intensity gradient constraint. Pentland uses a local approach in [11] based on the local sphericity assumption. However, they too have their limitations. Most minimization approaches have a tendency to be slow. Furthermore, standard variational algorithms may not reconstruct a surface from noisy images even after thousands of iterations [2].

Other shape recovery methods obtained very good results: photometric stereo [13], stereopsis, moving light source, structured light. These methods require multiple images often obtained under controlled conditions. Photometric stereo uses multiple images of the same object taken under different lighting conditions. The multiple illumination setup creates a system of irradiance equations which are used to recover the normal map (and albedo). Binocular (polyocular) stereo does not typically impose any restrictions on illumination, but requires capturing a scene from multiple viewpoints using at least two cameras. It tries to identify features in two or more images that are projections of the same entity in the 3D world. Structured light uses pictures of objects illuminated by a pattern of light. The camera senses the result as a grid distorted by the surface structure and its pose. Thus, although these shape recovery methods do not have the same constraints as SFS methods, they too have their inherent limitations.

Our methodology, Shape from Isophotes, is focusing on overcoming some of the shortcomings of SFS methods. More specifically, Shape from Isophotes avoids differentiation which results in improved (pixel level) accuracy. Unlike most of the previous methods, it is not gradient descent based and can be applied on piecewise smooth surfaces. It also explicitly addresses complications that may arise from brightness quantization errors. Our technique is not without limitations. Like other SFS methods, we too assume single distant point light source and orthographic projection.

The Shape from Isophotes (SFI) method is based on the close relationship between isophotes (regions of constant brightness) and surface normals [9, 10]. It initially directly recovers a small number of surface normals either on occluding contours or on singular points, in general on any pixel where a surface normal estimate can be directly obtained from the image. We then use the structure of isophote regions in an image to recover the remaining surface normals. Specifically, our method is composed of 2 parts: a) the method that deals with surface

normals at the border of isophote regions, which we will refer from now on as *the border method* and b) the method that propagates the surface normal information within an isophote region which we call *the interior method*. The border method calculates new values for the surface normal when there is a change in the image brightness between adjacent pixels, the interior method chooses the propagation direction for a known surface normal as long as there is no change in the image brightness.

## 2. OVERVIEW OF SHAPE FROM ISOPHOTES METHOD

### 2.1 Intensity Gradients and Curves of Steepest Descent

Many SFS algorithms [1, 3, 5, 8] use the direction of steepest descent, in recovering the surface normals. This principle states that if a step is taken in the image plane in a direction parallel to the gradient of the reflectance map, the corresponding step in gradient space is parallel to the gradient in the image. For rotationally symmetric reflectance maps, the direction of intensity gradient is also the direction of steepest descent [6]. However, these algorithms may fail to orient the surface normal correctly, particularly in regions where different surfaces may result in similar intensity gradients (for a graphic representation of this problem see figure 2). The effect is more pronounced when surface orientation is recovered based on local information.

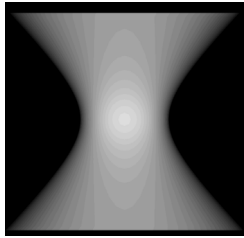


Figure 1. Synthetic image of a hyperboloid, Lambertian surface, illuminated by a distant point light source aligned with the optic axis.

Consider, for example a hyperboloid Lambertian surface, illuminated by a single distant light source aligned with the optic axis (see fig. 1). We use the notation  $(p,q)$  for the gradient of the surface.  $p$  is the slope of the surface with respect to the X-axis, i.e.  $p = \partial f(x,y) / \partial x$  while  $q$  is the slope of the surface with respect to the Y-axis, i.e.  $q = \partial f(x,y) / \partial y$ . Assume that the reflectance map  $R(p,q)$  has a unique isolated maximum at  $(p_0,q_0)$ , which means  $R(p,q) < R(p_0,q_0)$  for all  $(p,q) \neq (p_0,q_0)$  where  $R(p,q)$  is the reflectance map of the surface. Assume that at some point  $(x_0,y_0)$  in the image, the image irradiance  $E(x_0,y_0) = R(p_0,q_0)$ . This point is called a singular point and the gradient  $(p,q)$  at this point is uniquely determined to be  $(p_0,q_0)$  [6]. In our example, the singular point is at the centre of the image. The isophotes close to the singular point are almost circular. Still the surface is far from being rotationally symmetric. This suggests that there are cases when the characteristic curves methods may produce erroneous results. For instance, as shown in fig. 3, a characteristic strips method can lead to incorrect normals during propagation, even though it starts with accurate normal recovery at the singular point.

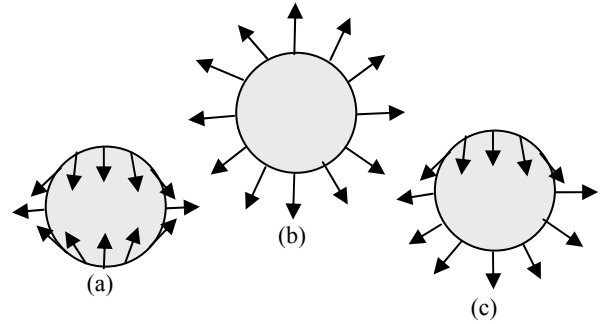


Figure 2. Three possible surface normal orientations on a singular region border

In fact, the singular point is often a singular region in images, due to brightness quantization, and most of its normals are neither identical, nor parallel to the incident light direction. Figure 2 graphically demonstrates a few possible normal orientations at the border of the singular region. The normals' directions inside the singular region are close enough to the light direction so that the whole region has maximum brightness. The propagation methods often approximate the region around the singular point with a spherical cap.

Characteristic strips methods are particularly sensitive in surface recovery in hyperbolic points, partly because they propagate normal information along the direction of intensity gradients. In order to overcome this, we decoupled the surface normal recovery computation from the propagation process. Our method, Shape from Isophotes, does not use the direction of steepest descent. More specifically, the surface normal recovery computation is done during the border method phase (see section 2.2) and the propagation during the interior method phase (see section 2.3).

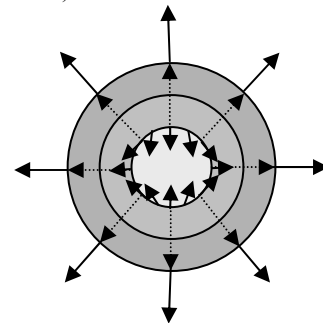


Figure 3. Characteristic strips (in dotted line).

Figure 4 shows the expected outcome of Shape from Isophotes for the same example of singular region. The solid arrows represent normals, the dotted lines the propagation path; the grey areas are isophote regions and the lines between them the borders between the isophote regions. The singular region has surface normals on the border similar to those in fig. 2(a).

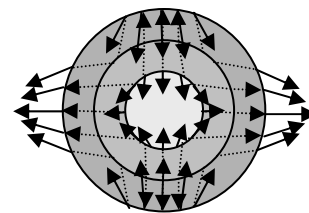


Figure 4. Shape from isophotes method.

## 2.2 Surface Normals at the Border of Isophote Regions

Consider two infinitesimally small planar surface patches  $p_1$  and  $p_2$  such that they correspond to image patches close to the isophote border which also lie on different sides of the border. Assume that we know the normal  $\mathbf{n}_1$  to the surface at a point  $P_1$  inside the surface patch  $p_1$ .  $P_1$  is adjacent to the border with the other isophote region. Then there is enough information to find the normal  $\mathbf{n}_2$  at the point  $P_2$  inside the surface patch  $p_2$ .

Let  $\mathbf{n}$  be the normal to the plane  $p$  which is perpendicular to the image plane and tangent to the isophote border (see figs. 5, 6, and 7). Then the normals  $\mathbf{n}_1$ ,  $\mathbf{n}_2$  and  $\mathbf{n}$  are coplanar, being normals to three planes whose intersection is a line.  $\mathbf{n}_1$  and  $\mathbf{n}$  constraint  $\mathbf{n}_2$ . Let  $S_2$  be the set of possible surface normal for patch  $p_2$  (see fig. 7). Since  $\mathbf{n}_2$  must be coplanar to  $\mathbf{n}_1$  and  $\mathbf{n}$ , there is a very small solution space for  $S_2$ . For example, for a Lambertian surface, the normals  $\mathbf{n}_1$  and  $\mathbf{n}$  must lie on a cone centred at the light source direction  $(p_s, q_s)$ . Then we can find the possible  $\mathbf{n}_2$  values by applying the co-planarity constraint to  $S_2$ .

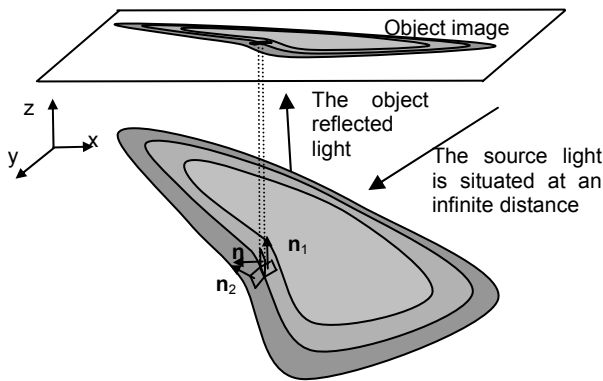


Figure 5. The image formation and the patch-plane correspondence. An object, its image, the isophote regions, the  $p_1$  and  $p_2$  patches, the  $p$  plane and the  $\mathbf{n}_1$ ,  $\mathbf{n}_2$  and  $\mathbf{n}$  normals.

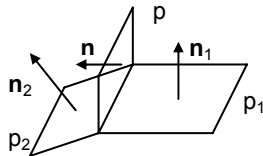


Figure 6.  $\mathbf{n}_1$ ,  $\mathbf{n}_2$  and  $\mathbf{n}$  are coplanar if the planes intersect on a line. The  $p_1$  and  $p_2$  patches, the  $p$  plane and the  $\mathbf{n}_1$ ,  $\mathbf{n}_2$  and  $\mathbf{n}$  normals isolated

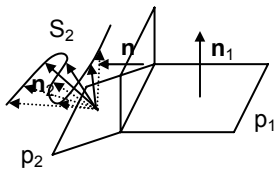


Figure 7. The intersection between  $S_2$  (the set of possible normals for the brightness of the point  $P_2$  and light direction) and the plane  $(\mathbf{n}_1, \mathbf{n})$  gives three solutions in this particular case.

However, the only feasible  $\mathbf{n}_2$  values must lie on the intersection of the cone with the plane that contains  $\mathbf{n}_1$  and  $\mathbf{n}$ . Then 0, 1 or 2 solutions are obtained. Normally, 0 solutions should never be obtained. If 0 solutions are obtained, the

starting normal had the wrong value and one should restart the computation with a different starting normal value. 1 solution is obtained inside a singular region. 2 solutions are obtained everywhere else. In practice, quantization errors make obtaining 0 solutions possible even if there should be 2 very close solutions. We chose to stop the propagation if the solutions were close to each other. In conclusion, by using our border method, we can estimate the surface normals at a pixel bordering an isophote region, once the normal at the other side of the border is known.

## 2.3 Surface Normals within an Isophote Region

Once a normal of an isophote region is known we can propagate that information inside an isophote region. We assume that locally the isophote is a developable surface with generator line  $L'_0$ . We propagate the surface normal information along the generator line or its approximation since that is the direction of minimal change. For approximately Lambertian surfaces it suffices to propagate along the plane of incidence. The plane of incidence at a point  $P$  is the plane defined by the incidence beam and the surface normal at point  $P$  (see fig. 8).

If the intersection between the incidence plane and the surface is a line, then it is the generator line  $L'_0$ . However, brightness quantization can create isophote regions resulting in the loss of finer shading information which cannot be recovered. Though we can not recover the original object shape, we can still extract the shape of a polygonal object which approximates the original object shape. For the approximate polygonal object, the image isophotes correspond to the planes of the object. We need to find out the generator lines  $L'_0$  which generate these planes. The surface normal does not change along that line.

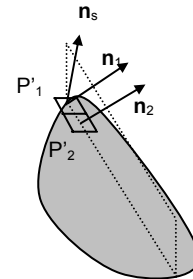


Figure 8. The construction for Surface Normals within an Isophote Region for a Lambertian surface

For diffuse surfaces in general, we can compute  $L'_0$  as follows. Assume that we choose three points  $\mathbf{n}_1$ ,  $\mathbf{n}_2$ ,  $\mathbf{n}_3$  in  $(p, q)$  space so that they lie on the locus of the same constant intensity (see fig. 9a). Each of these three points  $\mathbf{n}_i$  is represented by a plane  $p_i$  in  $(x, y, z)$  space (see fig. 9b). The intersection between any pair of these planes in  $(x, y, z)$  space is a line  $L'_i$  which is represented in  $(p, q)$  space by the line  $L_i$  that connects the corresponding points of those planes. The intersection between the planes  $p_1$  and  $p_2$  is represented by the line  $L_1$  which connects  $\mathbf{n}_1$  and  $\mathbf{n}_2$ . Now if  $\mathbf{n}_1$ ,  $\mathbf{n}_2$ ,  $\mathbf{n}_3$  are very close to each other, the lines that connect them are almost parallel to the tangent  $L_0$  to the curve in the middle point  $\mathbf{n}_2$ . This means that the intersections of the planes  $p_1$ ,  $p_2$  and  $p_3$  become almost parallel to the line  $L'_0$  in  $(x, y, z)$  that corresponds to that tangent. One can think of the planes  $p_1$ ,  $p_2$  and  $p_3$  as part of a developable surface whose generator is line  $L'_0$ .

Consider now all the points of the locus on which  $\mathbf{n}_1$ ,  $\mathbf{n}_2$  and  $\mathbf{n}_3$  lie. Each of the points on that locus corresponds to a plane in

(x,y,z) space. For each triplet of closely spaced consecutive points on the locus, one can apply the same logic. Thus, the normals on the entire locus corresponds to a developable surface whose generator is line  $L'_0$ . The entire developable surface is contained in the same isophote in our image.

The normals in other points of the same isophote region can be obtained either by interpolation, or by applying either the interior method or the border method to another known normal.

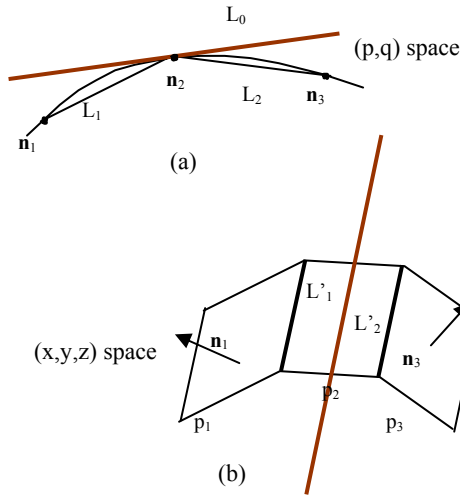


Figure 9. Three points on a curve both in a) (p,q) space and b) (x,y,z) space

## 2.4 Shape from Isophotes

In order to extract the surface normals at the whole surface, we combine both the border method and the interior method. On the isophote regions' borders the border method is applied, while in the interior of the isophotes regions' the interior method is applied. Both methods introduce some errors due to quantization, but the errors are within acceptable limits (see sections 4.1 and 4.2).

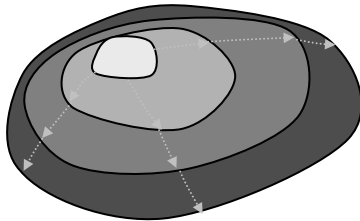


Figure 10. Shape from Isophotes can start at a singular point, as in this example, or from occluding contours.

Figure 10 shows the method applied to a simple convex object. Each different shade of grey represent a distinct isophote region. The propagation in this example started from the singular point. The arrows represent propagation directions.

Figure 11 shows the first 4 cycles of the method. The object was a sphere. The starting points are the border of the singular region. The upper row shows the propagation curves. The lower row shows the detected isophote region borders.

To summarize, the Shape from Shading algorithm is as follows:

1. Directly compute starting surface normals where available (e.g. at singular points or occluding contours)
2. Propagate away from the starting normals as follows:

If the current normal is adjacent to an isophote region apply the "border method, else apply the "interior method"

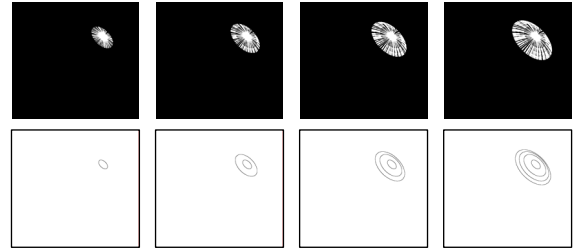


Figure 11. Hyperboloid, Lambertian surface, light perpendicular to the image.

## 3. EXPERIMENTS

In order to test the limitations of our method we first performed a series of test on synthetic images. That allows us to provide quantitative error measurements and examine the sensitivity of our method to noise. The objects' geometry and surface normals are known.

### 3.1 Synthetic Data

The sample images were created using a Lambertian surface, the error was calculated by averaging the angle between the calculated normal and the known normal at every point of the image that represents the object. The light source is a point light source at infinite distance. We tested the algorithm on two shapes: a hyperboloid and a cone. Two errors were calculated for each object: one before there was any interpolation done and one after the interpolation. Our first test (see figures 12 and 13) assumed ideal data, with no noise, so our only source of inaccuracies is quantization error. In order to test the sensitivity of our algorithm to noise, we added a random noise of +/-2 intensity values at each pixel (see figures 14 and 15).

Shape	Average error before interpolation	Average error after interpolation
Hyperboloid - noise free	1.502% (2.704°)	1.700% (3.060°)
Cone - noise free	1.665% (2.998°)	1.769% (3.184°)
Hyperboloid - noisy	2.719% (4.892°)	2.800% (5.039°)
Cone - noisy	2.134% (3.842°)	2.431% (4.376°)

Table 1. Average error for the Hyperboloid and Cone synthetic images

We started the propagation from the points on the occluding boundary. The albedo of the objects was known in advance. In each of the figures 12, 13, 14 and 15 the image that was analyzed is shown on the left, the recovered normal map is shown in the middle and an error image is shown on the right. The error image shows the error distribution on the surface. Darker areas have smaller errors, lighter ones bigger ones. The contrast was enhanced from the original image so that white corresponds to 100% error and black to 0% error for a better visibility. The biggest errors occur in the interpolated areas.

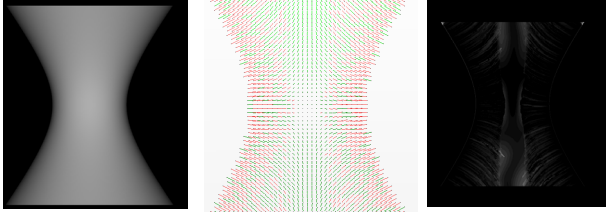


Figure 12. . Hyperboloid, Lambertian surface, light perpendicular to the image

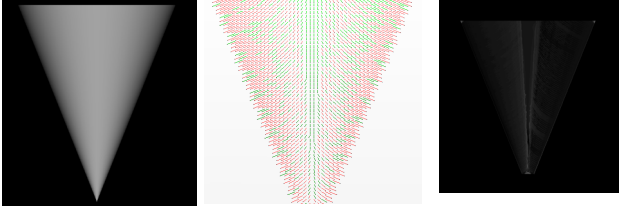


Figure 13. Cone, Lambertian surface, light perpendicular to the image

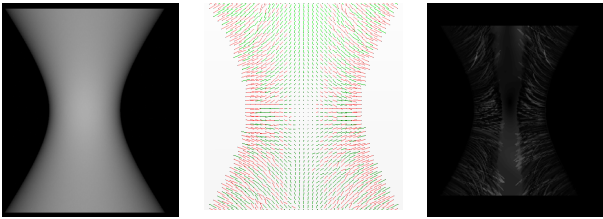


Figure 14. Hyperboloid, Lambertian surface, light perpendicular to the image

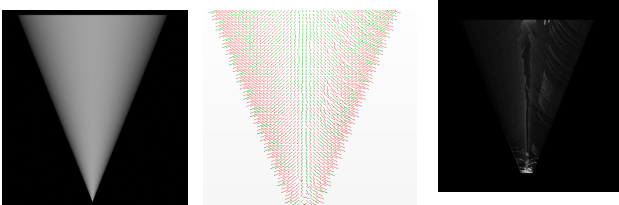


Figure 15. Cone, Lambertian surface, light perpendicular to the image.

### 3.2 Real Data

We also applied our algorithms on real data. The images were taken in a controlled environment. The objects were less than 10cm tall and the single light source was positioned about 50 cm away from the objects. The light source was positioned roughly above the XCDSX900 Sony camera. We used cross-polarization to eliminate specularities. We performed experiments on a white torus (fig. 16) and a billiard cue ball (fig. 17).

Shape	Average error before interpolation	Average error after interpolation
Billiard ball	3.813% (6.864°)	3.724% (6.704°)

Table 2. Average error for the Billiard ball image

Figures 16 and 17 show the images of the objects on the left and the recovered normals on the right. Since the billiard cue ball has known dimensions we performed error analysis on that object. As expected, the error is bigger than in the synthetic images, but an average error of less than 7° is a strong performance. The bigger error of the billiard ball sample is due to image noise, reflections, non-uniformity of the illuminant and inaccuracies in the position of the light source.

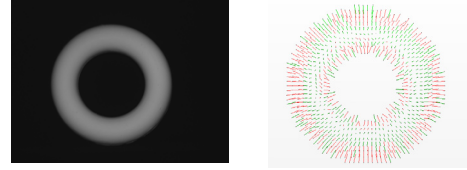


Figure 16. Torus

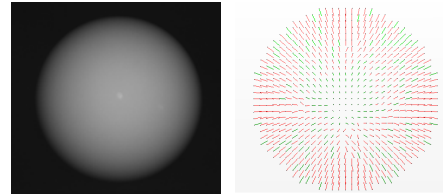


Figure 17. Billiard ball

## 4. LIMITATIONS

Our method has its limitations. Its accuracy depends on how accurately we can recover the surface normals at occluding contours. We tested the sensitivity of Shape From Isophotes to the accuracy of the estimates at the occluding contours for the hyperboloid synthetic image. Each normal at the occluding contour was perturbed by at most 1°, 2°, 3°, 4° and 5° accordingly. As expected the accuracy of the recovered normals was affected proportionally (see table 3), but the error in the recovered map was still below 18°. Furthermore, when the normals at occluding contours are error prone, the propagation paths are short and erratic (Figure 18a). Thus, one can detect that feature and associate a reliability measurement to each recovered normal.



Figure 18. Propagation curves for a) erroneous starting surface normals at the occluding contours and b) accurate starting surface normals at the occluding contours

Initial normals errors	Average Recovered normals error
0	1.465% (2.638°)
Between -1° and 1°	1.911% (3.441°)
Between -2° and 2°	3.460% (6.228°)
Between -3° and 3°	5.382% (9.687°)
Between -4° and 4°	7.921% (14.259°)
Between -5° and 5°	9.664% (17.396°)

Table 3. Average recovered normals error for an hyperboloid image when there are starting normals errors

Lastly, like other SFS methods, our technique, as is, is currently applicable to diffuse surfaces only. The surface generated by propagating from the starting curve might not cover the whole visible surface, so additional curves or some interpolation might be needed.

## 5. UNKNOWN LIGHT SOURCES

The light source does not need to be parallel to the viewer direction. Figure 19 shows normals recovered when the light is not parallel to the viewer direction, but is known. More specifically, in each of the synthetic images shown in figure 19 (from left to right) we moved the light source along the X-axis so that it would form a  $5.7^\circ$ ,  $11.3^\circ$  and  $16.7^\circ$  angle with the optic axis accordingly. The error in the recovered map is 1.616% ( $2.908^\circ$ ), 1.452% ( $2.613^\circ$ ) and 1.621% ( $2.918^\circ$ ) accordingly. After interpolation the error becomes 1.747% ( $3.144^\circ$ ), 2.172% ( $3.910^\circ$ ) and 2.447% ( $4.404^\circ$ ).

If our estimate of the light source position is erroneous, the normal map can still be recovered, but the larger our error in the light source position, the bigger our error in the recovered normal map. More specifically, for light source direction error of  $5.7^\circ$  the normal map error is 2.389% ( $4.301^\circ$ ), for  $11.3^\circ$  it is 4.407% ( $7.933^\circ$ ) after the initial light source direction error was again subtracted from the obtained normals. In this latter case the coverage was reduced to one side of the object and the strips were looking chaotic (figure 18a).

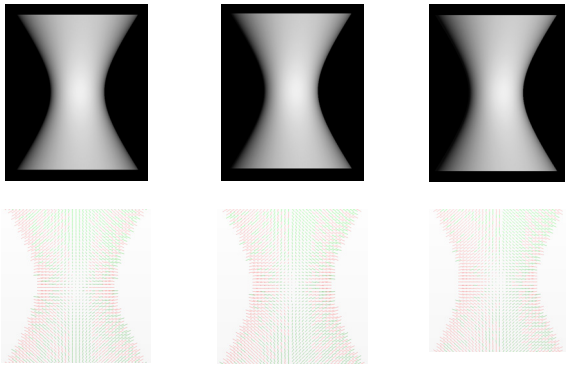


Figure 19. Hyperboloid, the source light comes from the right  $5.7^\circ$ ,  $11.3^\circ$  and  $16.7^\circ$

One can take advantage of the localized irregularities in the propagation direction and use them for iteratively improving the light source estimate. For example, the following algorithm could be used for detecting the light source direction, starting from an initial light source estimate:

1. Calculate starting normals using the light source direction
2. Calculate the normal map
3. Check strip coverage.
4. If the strip coverage contains erratic strips, move the light source toward the opposite direction of the object region which contains those strips and go to 1. Otherwise end the algorithm and keep the recovered light direction.

## 6. CONCLUSIONS

We developed a new Shape from Shading method that uses the image isophotes in recovering surface normals. Unlike minimization methods it does not suffer from numerical instabilities and because the propagation direction is decoupled from the gradient direction it is less error prone than characteristic strip methods in areas where the gradient is zero. Our quantitative error analysis showed an improved performance with average error of less than  $7^\circ$ . The errors are attributed to noise and to the fact that real images do not fully satisfy the simplifying assumptions of our theory (i.e. inter-

reflections, not truly distant light sources, etc.). Future work includes experiments using complex surfaces and relaxing more initial conditions. We are currently investigating isophote based techniques for iteratively estimating the light source direction and the normal map. We also want to expand our method to work with more complex reflectance maps, i.e textured surfaces and surfaces with specularities and shadows.

## 7. REFERENCES

- [1] M.Bichsel and A.P.Pentland, "A Simple Algorithm for Shape from Shading" *IEEE Proc. Computer Vision and Pattern Recognition*, pp. 459-465, 1992.
- [2] Paul Dupuis, John Oliensis, "Direct Method For Reconstructing Shape From Shading", *Proc. SPIE Conf. 1570 on Geometric Methods in Computer Vision*, pp. 116-128, July 1991.
- [3] Paul Dupuis, John Oliensis, "Direct Method For Reconstructing Shape From Shading", *IEEE Proc. Computer Vision and Pattern recognition*, pp. 720-721, June 1993.
- [4] R.T.Frankot and R.Chellappa, "A Method for Enforcing Integrability in Shape from Shading Algorithms", *IEEE Trans. Pattern Analysis and Machine Intelligence*, vol. 10, pp 439-451, 1988.
- [5] B.K.P. Horn, "Shape from Shading: A Method for Obtaining the Shape of a Smooth Opaque Object from One View", *PhD thesis, Massachusetts Inst. Of Technology*, 1970.
- [6] B.K.P. Horn, *Robot Vision* MIT Press, Cambridge, MA, 1987.
- [7] B.K.P. Horn, "Height and Gradient from Shading", *Int'l Journal of Computer Vision*, pp 37-75, 1989.
- [8] R.Kimmel and A.M.Bruckstein, "Tracking Level Sets by Level Sets: A Method for Solving the Shape from Shading problem", *Computer Vision and Image Understanding*, vol. 62, pp 47-58, July 1995.
- [9] J.J.Koenderink and A.J. Van Doorn, "Photometric Invariants Related To Solid Shape", *Journal of Modern Optics*, July 1980, vol. 27, no. 7, pp. 981-996
- [10] Jan J.Koenderink, "What does the occluding contour tell us about solid shape?", *Perception*, 1984, vol. 13, 321-330
- [11] A.P.Pentland, "Local Shading Analysis", *IEEE Trans. Pattern Analysis and Machine Intelligence*, vol. 6, pp. 170-187, March 1984.
- [12] Ariel Tankus, Nir Sochen, Yehezkel Yeshurun, "A New Perspective [on] Shape-from-Shading" *Proceedings of the Ninth IEEE International Conference on Computer Vision - Volume 2, 2003*.
- [13] Robert J. Woodham, "Photometric method for determining surface orientation from multiple images", *Optical Engineering*, January/February 1980, vol. 19 No.1
- [14] Ruo Zhang, Ping-Sing Tsai, James Edwin Cryer, and Mubarak Shah, "Shape from Shading: A Survey", *IEEE Trans. Pattern Analysis and Machine Intelligence*, vol.21, NO.8, August 1999.
- [15] Q.Zheng and R.Chellappa, "Estimation of Illuminant direction, Albedo, and Shape from Shading" *IEEE Trans. Pattern Analysis and Machine Intelligence*, vol. 13, no. 7, pp. 680-702, July 1991.